

Metal-terminated Graphene Nanoribbons

Yan Wang, Chao Cao, and Hai-Ping Cheng

Department of Physics and Quantum Theory Project, University of Florida, Gainesville, Florida 32611, USA

We have investigated structure, electronic, and magnetic properties of metal-terminated zigzag graphene nanoribbons (M-ZGNRs) by first-principles calculations. Two families of metal terminations are studied: 1) 3d-transition metals (TM) Fe, Co, and Ni; and 2) noble metals (NM) Cu, Ag, and Au. All systems have spin-polarized edge states with antiferromagnetic (AFM) ordering between two edges, except Co-ZGNRs and Ni-ZGNRs which exhibit negligibly small energy differences between AFM and ferromagnetic (FM) states with the given ribbon width. In the AFM state the TM terminations transform semiconducting ZGNRs into metallic ones, while the band gap remains in ZGNR with NM terminations. Ferromagnetic states of M-ZGNRs with TM terminations show a high degree of spin polarization at the Fermi energy. We predict a large magnetoresistance in Fe-ZGNR junctions with a low, uniform magnetic switching field.

PACS numbers: 73.22.Pr, 75.47.-m, 71.15.Mb

I. INTRODUCTION

Giant magnetoresistance (GMR)^{1,2} and tunneling magnetoresistance (TMR) effects³⁻⁷ in spin-valves and magnetic tunnel junctions have been the focus of spintronics studies in the past two decades. Conventional GMR and TMR devices, based on inorganic multilayered structures whose critical element is a sandwich of two magnetic layers separated by non-magnetic metallic or insulating layers, exhibit a large change in conductance when the orientation of the magnetic layers is changed from parallel (P) to antiparallel (AP). The magnetic layers are usually made of transition metal ferromagnets, which gives a high spin polarization at the Fermi energy.

Graphene nanoribbons (GNRs) with armchair (AGNR) or zigzag (ZGNR) edges⁸⁻¹², a novel organic material system produced by cutting graphene along two high-symmetry crystallographic directions, have recently attracted attention in spintronics. ZGNR is predicted to be a semiconductor with spin-polarized electronic states localized on the two edges that are individually ferromagnetically (FM) ordered but antiferromagnetically (AFM) coupled to each other through the graphene backbone¹³. Son *et al.*¹⁴ show that ZGNRs become half-metallic when an external transverse electric field is applied across the edges. Kim *et al.*¹⁵ propose a spin-valve based on a ZGNR connected by two ferromagnetic electrodes using a local magnetic field to switch the magnetization of one of the electrodes. Very recently a magnetoresistance device based on the transformation from the semiconducting state to the metallic state of the ZGNR has been proposed by Muñoz-Rojas *et al.*¹⁶; an estimated 200 T magnetic field is required to switch the AFM to the FM state at room temperature. Although these work demonstrate convincingly that spin-polarization and magnetoresistance can be realized using ZGNRs, the large magnitude of the electric field required to close the bandgap, the need of local magnetic control or a huge magnetic field, and small spin correlation length due to the lack of magnetic anisotropy in ZGNRs¹⁷ are serious limiting factors for future applications. Moreover, the predicted magnetic states in ZGNRs have not been experimentally observed so far.

Most of the theoretical studies on GNRs for spintron-

ics applications so far only address ribbons with hydrogen terminations¹⁴⁻¹⁶. Recent experiments have shown that graphitic surface curvature can be used as constraint and guide in which metal clusters aggregate to form linear islands^{18,19}. The presence of metal atoms adsorbed on the graphene²⁰⁻²³ or GNR²⁴ changes its electronic and magnetic properties and thus is certainly of great interest in physics.

In this paper we show that hybrid metal-terminated ZGNRs (M-ZGNRs) can be excellent candidate for spintronic applications. We studied various M-ZGNRs with terminations of 3d transition metals (TM) Fe, Co, Ni and noble metals (NM) Cu, Ag, Au using first-principles calculations. Compared with hydrogen terminated ZGNR (H-ZGNR), the TM and NM terminations lead to drastically different and unexpected effects in the structural, electronic and magnetic properties of the ribbon. A very large spin polarization is predicted for M-ZGNR with TM terminations in FM state. We propose a new type of junction with a low, uniform magnetic switching field that utilizes the electronic properties of M-ZGNRs, for which a magnetoresistance value as high as 200% can be obtained.

II. COMPUTATIONAL METHODS

The electronic structure calculations are performed using density functional theory (DFT) implemented in the PWSCF code²⁵. Each M-ZGNR is simulated within a supercell geometry containing two pristine ZGNR unit-cells with 40 C atoms and 4 metal atoms at two edges. Ultrasoft pseudo-potentials with kinetic energy cutoff of 500 eV are employed in all simulations. For the exchange and correlation functional we used the Perdew-Burke-Ernzerh generalized gradient approximation (GGA)²⁶. A vacuum layer of 15 Å is used between two edges and of 15 Å between two graphene planes to prevent interaction between adjacent images. Brillouin-Zone sampling uses a grid of 12 Monkhorst-Pack²⁷ k -points along the periodic direction of the ribbon. The optimization of atomic positions proceeds until the force on each atom is less than 0.01 eV/Å.

The transport calculations of the proposed Fe-ZNGR magnetic junction are performed by using the TRANSIESTA code³⁷, which is based on nonequilibrium Green's function

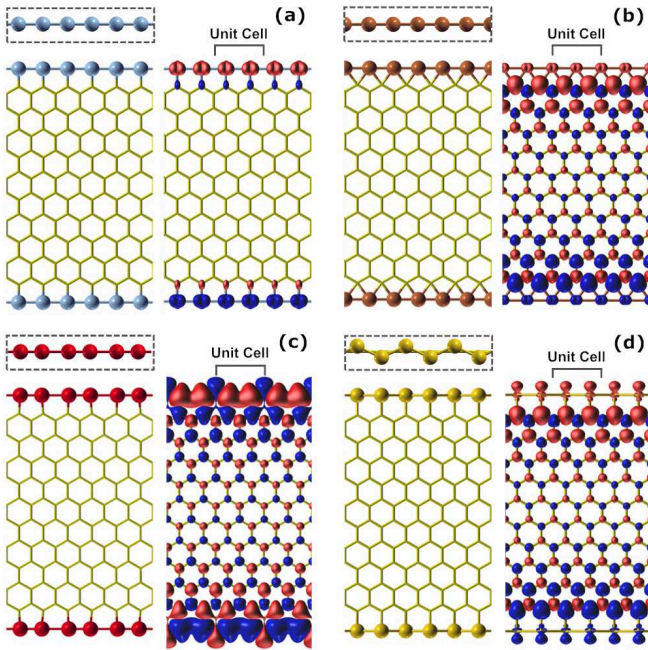


FIG. 1: (Color online). Four types of metal-terminated ZGNR: (a) Ni-ZGNR as linear A type (LA); (b) Cu-ZGNR as linear B type (LB); (c) Fe-ZGNR as dimerized linear type (DL); (d) Au-ZGNR as zigzag type (ZZ). The atomic configuration appears on the left, and on the right the corresponding spin density ($\rho = \rho_\alpha - \rho_\beta$) isosurfaces of the M-ZGNRs. The red (grey) and the blue (dark) isosurfaces denote $\pm 0.007 |e|/\text{\AA}^3$, respectively. The dashed box shows the edge view.

formalism and DFT as implemented in the SIESTA package³⁷. In order to reproduce the correct band structure of the lead, it is necessary to use double- ζ basis with polarization for Fe atoms, while single- ζ basis with polarization is sufficient for C atoms. The equivalent plane-wave cutoff for the real-space grid of 150 Ry is used in throughout the calculations. Current-voltage characteristics within small bias are calculated from the transmission coefficient $T(E)$ using $I = \int T(E)[f(E - \mu_L) - f(E - \mu_R)]dE$. The magnetoresistance can therefore be calculated via $MR = (I_P - I_{AP})/I_{AP}$.

III. RESULTS AND DISCUSSION

A. Structure, electronic, and magnetic properties

To determine the lowest-energy structures of the M-ZGNR, first we carried out structural relaxations for four possible termination configurations: the linear A type (LA), the linear B type (LB), the dimerized linear type (DL), and the zigzag type (ZZ), as shown in Fig. 1. Both edges of the ribbon have the same configuration for all systems. The calculated ground-state configurations as well as energetic and electronic properties are summarized in Table I. We find that for all cases the metal atoms bond strongly with edge carbon atoms, though the bonding configurations are quite different from one another, as shown in Fig. 1. For M-ZGNRs with Co and Ni ter-

minations, the relaxed structures are LA type. For Cu-ZGNR the most favorable structure is LB type, which is 0.98 eV/unit-cell more stable than the LA type structure, in good agreement with the result of Wu *et al.*²⁸. The Fe atoms dimerize at the edge of Fe-ZGNR due to the Peierls distortion²⁹. The most favorable structures for Ag-ZGNR and Au-ZGNR are ZZ type, with a metal-metal distance larger than the length of pristine ZGNR unit-cell. The binding energies E_b of the metal atom in M-ZGNRs, defined as $E_b = (E_{M-ZGNR} - E_{ZGNR})/4 - E_M^{\text{atom}}$, and the formation energy of the metal chain, $E_M^{\text{chain}} = E_M^{\text{chain}}/2 - E_M^{\text{atom}}$, are shown in Table. I. The large differences between E_b and E_M^{chain} indicate a large direct binding between the metal and carbon atoms at the ribbon edge. Bader analysis based on the real-space-charge density³⁰ for the M-ZGNRs shows charge transfer from metal atom to C atom for all cases. The amounts of charge transfer for Au-ZGNR and Ag-ZGNR are 0.08 and 0.19 $|e|/\text{metal-atom}$, respectively. Such a difference can be important for nanocatalysis.

For each M-ZGNR considered, the ground state has FM spin ordering of the metal atoms at each edge, while AFM order between the two edges is favored over FM, similar to H-ZGNRs and ZGNRs without H-passivation¹³. AFM coupling of the two edges is energetically more stable due to the indirect RKKY exchange interaction as a result of the bipartite lattice³¹, since the metal terminations always stand at the opposite sublattices at the two edges. For Fe-ZGNRs, the energy difference ΔE between the FM and AFM states increases with decreasing ribbon width³² due to increased interaction between enhanced spins in inner C sites inside the ribbon. Without the ribbon host the two Fe chains can only show direct FM exchange coupling through vacuum, and the calculated ΔE of the two Fe chains becomes less than 0.1 meV/ \AA when the distance is larger than 8 \AA . Nonetheless, as shown in Table. I, the ΔE for all M-ZGNRs are less than that of H-ZGNR, indicating a relatively small effective magnetic coupling between two edges, especially for TM terminations.

In general, the total magnetic moment of the system comes mostly from the metal atoms and their nearest-neighbor C atoms at the M-ZGNR edges. For TM-ZGNRs, the edge C atom presents magnetization antiparallel to the nearby TM atom. For Co-ZGNR and Ni-ZGNR in particular (see Fig. 1) the magnetic moments of the ribbon become more localized on the metal atoms at the edges compared to the inner C atoms in the ribbon, which leads to a negligibly small exchange energy shown in Table. I. For NM-ZGNRs, the metal atom shows magnetization parallel to that of the neighboring C atom at the edge, of order 0.01 $\mu_B/\text{metal-atom}$, mainly due to the proximity effect. The large difference between magnetic moments in TM and NM terminations reflects their different physical origins. In TM-ZGNRs, the relatively large moments of TM atoms come from unfilled d -shells and the TM-C covalent bond reduces the number of unpaired d -electrons, giving a reduced moment compared to the freestanding TM atom or monoatomic chain. For Cu, Ag and Au terminations with filled d -shells, the s valence electron saturates the dangling σ bonds similar to the hydrogen terminations in H-ZGNRs. The proximity-induced local magnetic moments for Cu, Ag, Au atoms are negligible, but the total edge moments of about 0.3

TABLE I: Structural, energetic and electronic properties of M-ZGNR. Columns show: metal termination, structures, metal-metal (d_{M-M}) and metal-carbon (d_{M-C}) bond length (in Å), the binding energy E_b and the formation energy of the metal chain $E_{\text{formation}}^{\text{chain}}$ (in eV per metal atom), energy difference $\Delta E = E_{\text{FM}} - E_{\text{AFM}}$ between the ferromagnetic and the antiferromagnetic state (in meV/unit-cell), charge transfer of the metal atom (in $|e|$) from Bader analysis, total magnetic moment m_{tot} of the ribbon in the FM state (in Bohr magneton μ_B per edge termination), local magnetic moment of the metal atom μ_M and its nearest-neighbor C atom μ_C (in μ_B), numbers of conduction bands crossing the Fermi level (n_{AFM} : the AFM state; n_{FM}^{α} and n_{FM}^{β} : majority and minority-spin in the FM state), and spin polarization P_{FM} of the ribbon at the Fermi energy in the FM state. Results for H-terminated ZGNR are also listed for comparison.

	structures	d_{M-M}	d_{M-C}	E_b	$E_{\text{formation}}^{\text{chain}}$	ΔE	Charge transfer	m_{tot}	μ_M	μ_C	n_{AFM}	$n_{\text{FM}}^{\alpha}(n_{\text{FM}}^{\beta})$	P_{FM}
Fe-ZGNR	DL	2.19(2.74) ^a	1.87	4.13	1.86	6.8	-0.31	2.19	2.47	-0.27	6	3(4)	82 %
Co-ZGNR	LA	2.46	1.82	4.26	1.79	1.3	-0.22	1.17	1.33	-0.11	10	3(7)	78 %
Ni-ZGNR	LA	2.46	1.80	4.44	1.74	<0.1	-0.19	0.18	0.23	-0.01	8	3(5)	55 %
Cu-ZGNR	LB	2.46	2.07	3.42	1.37	10.1	-0.41	0.26	0.01	0.29	0	1(1)	≈ 0
Ag-ZGNR	ZZ	2.74	2.15	2.38	1.20	7.8	-0.19	0.28	0.01	0.26	0	1(1)	≈ 0
Au-ZGNR	ZZ	2.71	2.07	3.00	1.65	11.5	-0.08	0.26	0.02	0.26	0	1(1)	≈ 0
H-ZGNR	LA	2.46	1.09	4.89	0.14	15.1	0.01	0.26	0.01	-0.30	0	1(1)	≈ 0

^aFe dimerization.

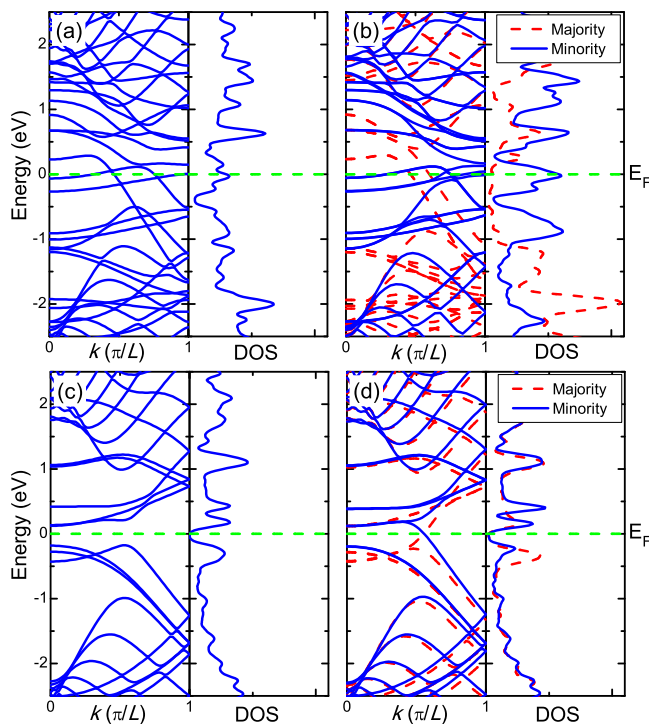


FIG. 2: (Color online). Energy band structures (left) and density of states (DOS, right, in states/eV) for the M-ZGNRs. (a): Fe-ZGNR in AFM state; (b): Fe-ZGNR in the FM state; (c) Au-ZGNR in the AFM state; (d): Au-ZGNR in the FM state. The dashed (red) and solid (blue) lines show the majority and minority spin, respectively. In the AFM state, majority and minority bands (DOS) coincide.

μ_B /metal-atom are very close to that of H-ZGNR. Although Mermin-Wagner theorem³³ excludes long-range order in 1D spin lattice model at finite temperature which would limit the dimension of devices based on H-ZGNRs to several nanometers at room temperature¹⁷, improvements can be expected in systems of M-ZGNRs by increasing the magnetic anisotropy as well as the spin correlation length.

The ground-state TM-ZGNRs are all metallic and the NM-

ZGNRs are all semiconductor. We show the band structures and density of states (DOS) of Fe-ZGNR and Au-ZGNR in Fig. 2. For Fe-ZGNR, both AFM and FM states are metallic. In the FM state, more flat bands of minority spin cross the Fermi level compared to those of the majority spin, resulting in a high spin polarization at the Fermi level, as can be seen in Fig. 2 (b). A detailed analysis of the projected DOS indicates that the states near the Fermi level are mainly from the Fe d orbital. Spin polarization P_{FM} can be calculated as $P_{\text{FM}} = |N_{\alpha} - N_{\beta}| / (N_{\alpha} + N_{\beta})$, where N_{α} (N_{β}) represents the DOS of majority (minority) spins at the Fermi energy. The P_{FM} of the Fe-ZGNR at E_F is about 82% which is much higher than that of bulk Fe^{34,35}. This implies that in the ballistic transport regime, the conductance of electrons with one type of spin is larger than the opposite spin. Similar to Fe-ZGNRs, the FM states of Co and Ni terminated ribbons also show high spin polarization, 78% and 55% respectively.

However, all studied NM-ZGNRs, have a bandgap comparable to that of the hydrogenated ribbon (0.32 eV) in the AFM ground-state. The band structure and density of states of Au-ZGNR as a typical case for NM-ZGNRs are displayed in Fig. 2 (c) and (d). In the FM metallic state the Au-ZGNR shows a large spin polarization only at the energies slightly away from the E_F . We also note that the band structure of NM-ZGNR is very sensitive to the edge structure. The metastable LA type of Au-ZGNR is metallic for both FM and AFM states.

B. Metal-terminated graphene nanoribbon junction

Our calculations of truncated Fe-ZGNRs provide an interesting result: if the transverse armchair edge is terminated by Fe, the strong magnetic coupling will align all edge spins in the same direction. Such highly spin polarized FM states can be useful in spintronics; in particular, a junction consisting of two TM-ZGNR leads separated by a spacer can operate as a magnetoresistance device. Fig. 3 (a) is a prototype multi-layer junction stacking three layers of Fe-ZGNRs. The center spacer can be a nonmagnetic metal such as Cr or Cu, since

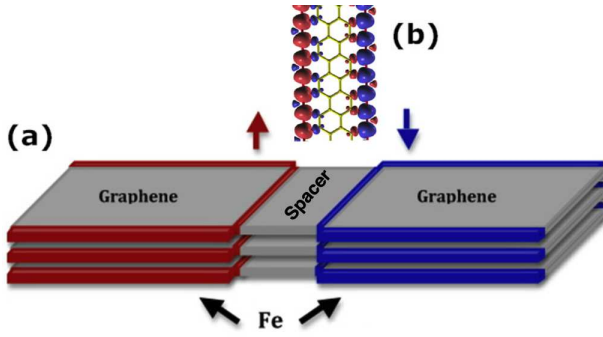


FIG. 3: (Color online). (a) Schematic figure of a multi-layer Fe-ZGNR/spacer/Fe-ZGNR junction prototype with antiparallel ground-state configuration. (b) Calculated ground-state (AFM) spin density isosurfaces of the Fe-AGNR with a width of 7.2 Å.

the behavior of the AFM exchange coupling between magnetic layers through a nonmagnetic spacer is well-known³⁶ and a GMR junction can thus be made; one can also use a small piece of non-conducting AGNR connected to the two leads via Fe chains, as the spacer which will provide a magnetoresistance junction. The key issue is the AP configuration being the ground state through the spacer: the junction can be switched to the P configuration under a uniform external magnetic field applied to both leads, without the need for a local magnetic field. A conductance difference between P and AP is in general expected. Our calculations show that the Fe-terminated two armchair edges favor either AFM or FM configurations depending on the width of the spacer. In Fig. 3 (b) we show an Fe-AGNR with a width of 7.2 Å which has an AFM ground-state that is 1.1 meV/Å lower than the FM state. AFM coupling of the two armchair edge states of the spacer can lead to an AP ground-state magnetic coupling between the two Fe-ZGNR leads. This energy difference can be tuned by increasing the thickness of the lateral Fe chain and by using multiple layers as shown in Fig. 3 (a). We also note that such a junction can be made by two Fe-AZGNR leads separated by a Fe-ZGNR spacer with similar function³⁹.

To illustrate the possible magnetoresistance, we have performed quantum transport calculations for a model magnetic tunnel junction based on two semi-infinite Fe-ZGNR leads. A 3.1 Å gap is set between two leads to represent the Fe-AGNR spacer. The spin-dependent current-voltage characteristics for small bias (linear response region) are calculated from the energy-dependent transmission coefficients in the ballistic tunneling regime. Large transmission differences are found near the Fermi energy, as shown in Fig. 4 (a). By comparing the current-voltage characteristics between P and AP configurations in Fig. 4 (b), we find a magnetoresistance up to 200% within the small bias region, which is comparable to the TMR ratio observed in conventional Fe/MgO/Fe sandwiched junctions^{6,7}. Negative magnetoresistance is also found in the region from 0 to 0.2 eV, as shown in Fig. 4 (c), primary due to the existence of several large peaks in the transmission of AP configuration which are very close to the Fermi energy.

Finally we discuss the operational conditions of our proposed magnetic junction of Fe-ZGNR/Fe-AGNR/Fe-ZGNR.

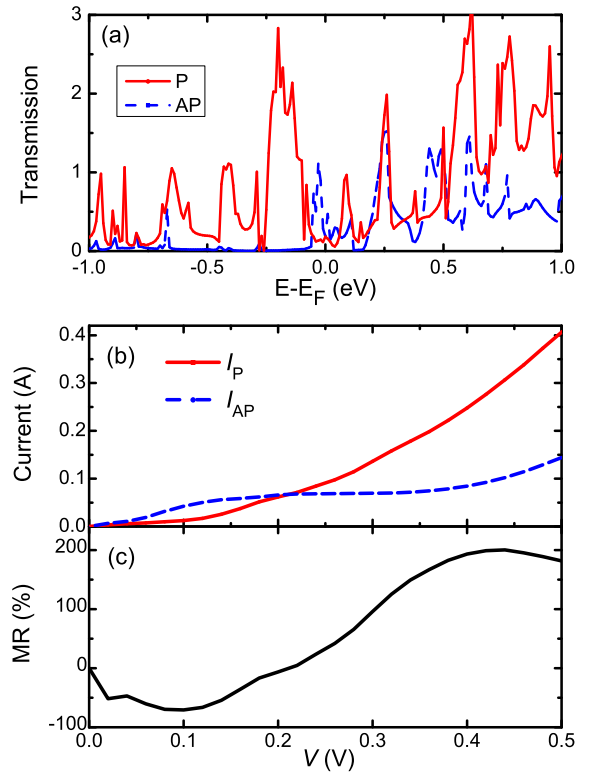


FIG. 4: (Color online). Transport properties for a model magnetic tunnel junction with two semi-infinite Fe-ZGNR leads separated by a 3.1 Å vacuum gap. (a) Energy-dependent transmission coefficients and (b) current-voltage characteristics within small bias region. The solid (red) and dashed (blue) lines represent the results for parallel (P) and antiparallel (AP) magnetic configuration of the two leads, respectively. (c) Calculated magnetoresistance (MR) as a function of bias voltage.

For a lead of infinite size any external field would switch the magnetization of the ZGNR lead. For a junction with finite-size leads, the critical switching magnetic field is defined as $B = \Delta E / g\mu_B M_{\text{tot}}$, where ΔE is the energy difference between P and AP configurations corresponding to the Zeeman energy splitting, M_{tot} is the total magnetic moment of the junction in the P configuration, $g = 2$ for graphene and $\mu_B = 0.058$ meV/T. A junction with two Fe-ZGNR leads of length 10 nm and a Fe-AGNR spacer 2.4 nm in length and 7.2 Å in width produces a ΔE of about 26 meV, which is comparable to room temperature kT . The junction with ideal edge termination of Fe atoms has a M_{tot} of 415 μ_B , thus resulting in a critical switching field as low as 0.54 T, which is much less than that of the junction proposed by Muñoz-Rojas *et al.*¹⁶. In experiments the possible formation of Fe wires of finite width at the Fe-ZGNR lead edges would enhance the total magnetization and thus further reduce the effective switching field. This junction shows a big advantage over the devices based on H-ZGNRs which mainly rely on ferromagnetic electrodes as well as local magnetic control¹⁵ or a huge switching magnetic field¹⁶. Current nano-size lithographic techniques can provide the basis for fabricating and patterning of such junctions.

IV. CONCLUSION

In summary, we have found that TM and NM terminated ZGNRs have completely different structures and magnetic properties. The TM terminations transform semiconducting ZGNRs to metallic, while NM termination does not affect the semiconducting nature of the ZGNR. ZGNRs with TM terminations and ferromagnetically coupled edges states show a high spin polarization at the Fermi energy. We propose a magnetic junction with low, uniform switching field using the Fe-ZGNRs as the ferromagnetic electrodes, and quantum transport calculations indicate a large magnetoresistance is possible in such junctions. Our results outline a roadmap to observe the magnetic order in graphene nanoribbon and hopefully stimulate experimental activities in the near future.

Note added in proof. In an extended study we have examined the ribbon width dependence of magnetic coupling between two edges of metal-terminated ZGNRs and AGNRs using projector augmented wave (PAW) potentials within DFT, and the results will be published elsewhere.

Acknowledgments

This work was supported by US/DOE/BES/DE-FG02-02ER45995. The authors acknowledge DOE/NERSC and the UF-HPC center for providing computational resources. C. Cao acknowledges support from NSFC (Grant No. 10904127).

-
- ¹ M. N. Baibich *et al.*, Phys. Rev. Lett. **61**, 2472 (1988).
 - ² G. Binasch, P. Grunberg, F. Saurenbach, and W. Zinn, Phys. Rev. B **39**, 4828 (1989).
 - ³ T. Miyazaki and N. Tezuka, J. Magn. Magn. Mater. **139**, L231 (1995).
 - ⁴ J. S. Moodera, L. R. Kinder, T. M. Wong, and R. Meservey, Phys. Rev. Lett. **74**, 3273 (1995).
 - ⁵ W. H. Butler, X.-G. Zhang, T. C. Schulthess, and J. M. MacLaren, Phys. Rev. B **63**, 054416 (2001).
 - ⁶ S. S. P. Parkin, C. Kaiser, A. Panchula, P. M. Rice, B. Hughes, M. Samant, and S.-H. Yang, Nat. Mater. **3**, 862 (2004)
 - ⁷ S. Yuasa, T. Nagahama, A. Fukushima, Y. Suzuki, and K. Ando, Nat. Mater. **3**, 868 (2004).
 - ⁸ K. Nakada, M. Fujita, G. Dresselhaus, and M. S. Dresselhaus, Phys. Rev. B **54**, 17954 (1996).
 - ⁹ M. Fujita, K. Wakabayashi, K. Nakada, and K. Kusakabe, J. Phys. Soc. Jpn. **65**, 1920 (1996).
 - ¹⁰ M. Y. Han, B. Ozyilmaz, Y. Zhang, and P. Kim, Phys. Rev. Lett. **98**, 206805 (2007).
 - ¹¹ B. Özyilmaz, P. Jarillo-Herrero, D. Efetov, D. A. Abanin, L. S. Levitov, and P. Kim, Phys. Rev. Lett. **99**, 166804 (2007).
 - ¹² X. Li, X. Wang, L. Zhang, S. Lee, and H. Dai, Science **319**, 1229 (2008).
 - ¹³ Y.-W. Son, M. L. Cohen, and S. G. Louie, Phys. Rev. Lett. **97**, 216803 (2006).
 - ¹⁴ Y.-W. Son, M. L. Cohen, and S. G. Louie, Nature **444**, 347 (2006).
 - ¹⁵ W. Y. Kim and K. S. Kim, Nature Nanotech. **3**, 408 (2008).
 - ¹⁶ F. Muñoz-Rojas, J. Fernández-Rossier, and J. J. Palacios, Phys. Rev. Lett. **102**, 136810 (2009).
 - ¹⁷ O. V. Yazyev and M. I. Katsnelson, Phys. Rev. Lett. **100**, 047209 (2008).
 - ¹⁸ M. Schmidt, N. Kébaïli, A. Lando, S. Benrezzak, L. Baraton, Ph. Cahuzac, A. Masson, and C. Bréchnignac, Phys. Rev. B **77**, 205420 (2008).
 - ¹⁹ A. F. Kemper, H-P. Cheng, N. Kébaïli, S. Benrezzak, M. Schmidt, A. Masson, and C. Bréchnignac, Phys. Rev. B **79**, 193403 (2009).
 - ²⁰ K. T. Chan, J. B. Neaton, and M. L. Cohen, Phys. Rev. B **77**, 235430 (2008).
 - ²¹ H. Jöhl, H. C. Kang and E. S. Tok, Phys. Rev. B **79**, 245416 (2009).
 - ²² A. V. Krasheninnikov, P. O. Lehtinen, A. S. Foster, P. Pyykkö, and R. M. Nieminen, Phys. Rev. Lett. **102**, 126807 (2009).
 - ²³ C. Cao, M. Wu, J. Jiang, and H.-P. Cheng, Phys. Rev. B **81**, 205424 (2010).
 - ²⁴ V. A. Rigo, T. B. Martins, A. J. R. da Silva, A. Fazio, and R. H. Miwa, Phys. Rev. B **79**, 075435 (2009).
 - ²⁵ P. Giannozzi, S. Baroni, N. Bonini, M. Calandra, R. Car, C. Cavazzoni, D. Ceresoli, G. L. Chiarotti, M. Cococcioni, I. Dabo, A. Dal Corso, S. Fabris, G. Fratesi, S. de Gironcoli, R. Gebauer, U. Gerstmann, C. Gougoussis, A. Kokalj, M. Lazzeri, L. Martin-Samos, N. Marzari, F. Mauri, R. Mazzarello, S. Paolini, A. Pasquarello, L. Paulatto, C. Sbraccia, S. Scandolo, G. Sclauzero, A. P. Seitsonen, A. Smogunov, P. Umari, R. M. Wentzcovitch, J. Phys.: Condens. Matter, **21**, 395502 (2009).
 - ²⁶ J. P. Perdew, K. Burke, and M. Ernzerhof, Phys. Rev. Lett. **77**, 3865 (1996).
 - ²⁷ H. J. Monkhorst and J. D. Pack, Phys. Rev. B **13**, 5188 (1976).
 - ²⁸ M. Wu, Y. Pei, and X. C. Zeng, J. Am. Chem. Soc. **132**, 5554 (2010).
 - ²⁹ R. E. Peierls, Quantum theory of solids. Oxford University Press, London (1955).
 - ³⁰ G. Henkelman, A. Arnaldsson, and H. Jónsson, Comput. Mater. Sci. **36**, 254-360 (2006).
 - ³¹ S. Saremi, Phys. Rev. B **76**, 184430 (2007).
 - ³² S. V. Ong, R. Robles and S. N. Khanna, Chem. Phys. Lett. **492**, 127 (2010).
 - ³³ N. D. Mermin and H. Wagner, Phys. Rev. Lett. **17**, 1133 (1966).
 - ³⁴ P. M. Tedrow and R. Meservey, Phys. Rev. B **7**, 318 (1973).
 - ³⁵ R. J. Soulen Jr., J. M. Byers, M. S. Osofsky, B. Nadgorny, T. Ambrose, S. F. Cheng, P. R. Broussard, C. T. Tanaka, J. Nowak, J. S. Moodera, A. Barry, J. M. D. Coey, Science **282**, 85 (1998).
 - ³⁶ P. A. Grünberg, Rev. Mod. Phys. **80**, 1531 (2008).
 - ³⁷ J. M. Soler, E. Artacho, J. D. Gale, A. García, J. Junquera, Pablo Ordejón and D. Sánchez-Portal, J. Phys.: Condens. Matter **14**, 2745 (2002).
 - ³⁸ M. Brandbyge, J. L. Mozos, P. Ordejón, J. Taylor, and K. Stokbro, Phys. Rev. B **65**, 165401 (2002).
 - ³⁹ The Fe-AGNR in the FM state also shows a large spin polarization at the Fermi energy, as confirmed by our calculation.